Uncertainties, complexities and possible forecasting of the volcán de Colima energy emissions (México, years 2013-2015) based on the fractal reconstruction theorem

Xavier Lana[1], Marisol Monterrubio-Velasco[2], Raúl Arámbula-Mendoza[3]

[1]Department of Physics, ETSEIB, Universitat Politècnica de Catalunya, Diagonal 647, 08028 Barcelona, Spain
[2]Department of CASE, Supercomputing Center, BSC-CNS, Eusebi Güell 1-3, 08034 Barcelona, Spain
[3]Centro Universitario de Estudios e Investigaciones de Vulcanología (CUEIV), Universidad de Colima, Av. Bernal Díaz del Castillo No. 340, Col. Villas San Sebastián, C.P. 28045, Colima, México

Correspondence to: Xavier Lana (francisco.javier.lana@upc.edu)

Abstract.

The effusive-explosive energy emissions process in a volcano is a dynamic and complex physical phenomenon. The importance of quantifying this complexity in terms of the physical and mathematical mechanisms that govern these emissions should be a requirement for deciding to apply a possible forecasting strategy with a sufficient degree of certainty. The complexity of this process is determined in this research by means of the reconstruction theorem and statistical procedures applied to the effusive-explosive volcanic energy emissions corresponding to the activity in the Volcán de Colima (western segment of the Trans-Mexican volcanic belt) along the years 2013-2015. The analysis is focused on measuring the degree of persistence, or randomness of the series; the degree of predictability of energy emissions; and the quantification of the degree of complexity and "memory loss" of the physical mechanism throughout an episode of volcanic emissions. The results indicate that the analysed time series depict a high degree of persistence and low memory loss, becoming the mentioned effusive-explosive volcanic emission structure a candidate to successfully apply a forecasting strategy.

Key-words: Volcan de Colima explosions, México, fractal reconstruction theorem, Hurst, Lyapunov and Kolmogorov exponents, possible forecasting and nowcasting strategies.

1 Introduction

A right forecasting of dangerous long drought episodes, high magnitude earthquakes or great volcanic emissions should be one of the main objectives on the scientific fields of climatology, seismology or volcanology to prevent disasters which could affect the environment and the human life. Several examples of forecasting algorithms could be cited, among them the nowcasting strategy (Rundle et al., 2016, 2017), the multifractal analysis in seismology (Monterrubio-Velasco et al., 2020),

the ARIMA process in climatic research (Lana et al, 2021), and neural algorithms (Lipton et al, 2015 and Lei, 2021) also useful to predict monthly rainfall. These cited algorithms systematically forecast the next episode taking into account a certain number of previous recorded data, being this number strongly associated with the characteristics of the physical mechanism. These forecasting results should be validated by previously analysing the degree of complexity and the "loss of

35 memory" of the physical mechanisms along the evolution of the physical process. In other words, how many previous data would be necessary for a right use of a forecasting algorithm and which could be the range of uncertainties on the predictions.

The database, Section 2, analysed in this research is the time series of explosive volcanic events (Vulcanian explosions) emitted by Volcán de Colima (Western segment of Trans-Mexican volcanic belt) during the years 2013-2015. A Vulcanian

40 explosion is an eruption where fragmented material is expulsed to the atmosphere, as result of an overpressure into the conduit or lava dome (Arámbula-Mendoza et al., 2018). The event releases energy in several ways, based on elastic, seismic, acoustic and thermal processes. The next explosion will occur when again the overpressure break again the impermeable cap. The Volcán de Colima has emitted many Vulcanian explosions, some of them with generation of Pyroclastic Density Currents (PDCs) until 5 km of runout (Arámbula-Mendoza et al., 2019). For these reasons, strategies for a right forecasting

45 of the mentioned Vulcanian explosions are important.

The reconstruction theorem (Section 3) is a mathematical strategy that allows quantify the degree of complexity in a time-series and it loss of memory, both required to validate a possible forecasting strategy (Dicks, 1999). Additionally, the nowcasting algorithm (Section 5), a statistical process developed by Rundle et al. (2016, 2017) to detect the risk of imminent high magnitude earthquakes, could be also applied to quantify the probability of an imminent high magnitude volcanic

50 emission. .

The main objective of this work is to detect the degree of difficulty for a forecasting of volcanic emissions associated with energies close to or exceeding 10^8 J. By means of the reconstruction theory (Diks, 1999) the complexity is measured by means of some parameters such as the persistence degree, the intensity of chaotic behavior of the system , and the "loss of memory" of the physical mechanism. Moreover, the statistical distribution of the effusive-explosive energy of these

55 emissions and their return periods are also analysed. The just mentioned nowcasting strategy is also taken into account to confirm future extreme emissions of energy. The results obtained after applying the reconstruction theorem, analysing the whole time series, 6 consecutive segments and 21 moving window data, are detailed in Section 4.

The most relevant results of the reconstruction theorem and their effects on forecasting algorithms are discussed in Section 6. Finally, the Section 7 (Conclusions), summarizes the most relevant results with respect to the expected success on preventing

60 volcanic energy emissions, based on forecasting and nowcasting processes.

2. Database

A time series of volcanic explosions, named as Vulcanian explosions (Bachtell Clarke and Esposti Ongaro, 2015) emitted by Volcán de Colima (Western segment of Trans-Mexican volcanic belt, years 2013-2015) (Arámbula-Mendoza et al., 2018) is analysed. Figure 1a depicts the histogram of the logarithm of the emitted energy. The dataset contains 6182 observations of the emissions equalling to or exceeding approximately 2×10^6 J accomplishing the Gutenberg-Richter law (Gutenberg and Richter, 1958) as shows Figure 1b.

Figure 2a describes the six segments to be analysed, where can be observed the highest explosions at the beginning of the first segment [$\log_{10}$(Energy)=8.2], third segment [$\log_{10}$(Energy)=8.4] and at the end of the series, out of the 6th segment [$\log_{10}$ (Energy)=8.9]. With the aim of analysing the whole set of volcanic emissions accomplishing the Gutenberg-Richter law, Figure 2b depicts two examples of moving window segments.

The statistical distribution of these emissions is analysed by means of the L-Skewness-Kurtosis formulation (Hosking and Wallis, 1997). The statistical analysis of these emissions shows that the complete series of emissions, including those not accomplishing the Gutenberg-Richter law, are well fitted to the Generalised Logistic, GL, function (Figures 3a and 3b). Additionally, three different empirical distributions of extreme emissions, equalling to or exceeding respectively 90%, 95% and 99% of data (Figure 3b), can be associated with the Generalised Extreme value, GEV, function. Figure 4 shows the evolution of these three expected extreme emissions with the increasing return periods (given in number of events equalling to or exceeding 90, 95 and 99% respectively). For instance, the expected values of emissions for the three percentage levels and return periods up to 200 extreme emissions fit quite well the theoretical evolution, with emissions close to 1.0×10^8 J, 2.0×10^8 J and 8.0×10^8 J for 90, 95 and 99% extreme distributions. This first approach to the possibility of very high explosions and the corresponding expected return period (number of extreme episodes before a very high extreme emission) would be quite similar to a nowcasting analysis, strategy proposed by Rundle et al. (2016, 2017) to detect the risk of imminent high magnitude earthquakes.

3. The reconstruction theorem

Previously to the reconstruction theorem (Diks, 1999) based on monofractal theory, the degree of randomness, anti-persistence or persistence of the analysed data is established taking into account the concept of the Hurst exponent (Turcotte 1997) which is defined as the exponent H of the power-law

$$\frac{R(\tau)}{S(\tau)} \propto \tau^H, \tag{1}$$

being R(τ) the range of the different chosen segments of length τ of a series and S(τ) the corresponding standard deviation. H close to 0.5 implies a strong randomness of the series. Conversely, H clearly lowering or exceeding 0.5 means anti-persistence or persistence, respectively. Consequently, the Hurst exponent offers a first point of view of the behaviour of the analysed series. It has to be also remembered that the Hurst exponent has to be coincident with a specific value of the generalised Hurst exponent, obtained by means of multifractal analysis (Kantelhardt et al., 2002) applied to the same series. The analysis of the monofractal structure of a series, by means of the reconstruction theorem (Diks, 1999), permits quantifying its complex forecasting by means of the following parameters:

-The necessary minimum number of nonlinear equations governing the physical mechanism, usually referenced as correlation dimension, $\mu(m)$, being m the reconstruction space dimension.

-The embedding dimension, d_E, the asymptotic value of the correlation dimension, with m theoretically tending to ∞.

-The Kolmogorov entropy, κ, which quantifies the loss of memory of the mechanism along the analysed physical process.

The reconstruction theorem process is based on generating a set of m-dimensional space vectors using the series {x(i)} of data :

$$Z(i)=x_i,x_{i+1},...,x_{i+m-1},i=1,...,n-m+1 \tag{2}$$

being n the length of the series, and the definition of the correlation integral in terms of the Grassberger–Procaccia formulation (Grassberger and Procaccia, 1983a, 1983b)

$$C(m,r)=\lim_{N\to\infty}\frac{1}{N^2}\sum_{i,j=1}^{N}H\left\{r-\|z(i)-z(j)\|\right\} \tag{3}$$

r being an Euclidean distance in the m-dimensional space and H{.} the Heaviside function. The correlation integral can be rewritten as

$$C(m,r)=A_m e^{-mk}r^{\mu(m)} \tag{4}$$

$$\log[C(m,r)]=\log(A_m)-mk+\mu(m)\log(r) \tag{5}$$

being K the Kolmogorov entropy exponent and A_m and $\mu(m)$ the correlation amplitude and the mentioned correlation dimension for every reconstruction dimension m. A confident quantification of $\mu(m)$ for every reconstruction dimension has

to be carefully computed, avoiding a very flat evolution of C(m,r) for small values of r, caused by the lacunarity (Turcotte, 1997), and the saturation of C(m,r) for the highest values of r. With respect to the quantification of the Kolmogorov entropy, K, by using equation 5, naming $\mu(m)$ the term $log\{C(m, r)\}-\mu(m)log(r)$, and after obtaining $\alpha(m)$, the equation 5 becomes

$$\alpha\left(m\right)=\log\left(A_m\right)-mK \tag{6}$$

Equation 6 is characterised by an almost constant value of $\log\left(A_m\right)$ for high reconstruction dimensions m. Consequently, a very accurate value of the Kolmogorov coefficient K could be obtained by a linear regression in terms of equation 6, but only for the mentioned set of the highest reconstruction dimensions m. The same set of m-dimensional space vectors permits the computation of the Lyapunov exponents λ_i, (i=1,…m) (Eckmann et al., 1986; Stoop and Meier, 1988; Wiggins, 2003) which quantify the intensity of chaotic behavior of a system specially the first λ_1 exponent) when the results, forthcoming volcanic emissions at the present case, have been estimated by means of some forecasting algorithm. Additionally, the Kaplan-Yorke dimension, D_{KY}, (Kaplan and Yorke, 1979)

$$D_{KY}=l_0+\left|\frac{1}{\lambda_{l0+1}}\left|\sum_{j=1}^{l_0}\lambda_j\right.\right. \tag{7}$$

,with l_0 the maximum number of Lyapunov exponents in decreasing order accomplishing

$$\lambda_1+\lambda_2+...+\lambda_{l_0}\geq0, \tag{8}$$

quantifies the fractal dimension of the nucleus around of which the consecutive m-dimensional vectors describe the corresponding orbital trajectories. In short, the highest the value of D_{KY}, more complex will be to establish the forthcoming value of the analysed physical problem.

4. Results

4.1 The Hurst exponent.

The results of the Hurst exponent for the whole series and the six data segments is described in Figures 5a and 5b, being obtained a clear sign of persistence for the complete series of Vulcanian explosions, with H exceeding a value of 0.7, a moderate persistence for the first, second, fourth and fifth segments, a smooth increase of H from the fifth to the sixth segment and a clear persistence (H > 0.70) for the third segment. This third clear persistence is detected for a data segment including the second highest energy emission (Figures 2a and 2b). Conversely, the lowest Hurst exponents for the

first, second, fourth and fifth segments are characterised by more moderate emissions of energy. Finally, the increase of H for the sixth segment could be caused by the imminence of the highest energy, an emission immediately after this data segment. A more detailed evolution of the Hurst exponent is described by the 21 moving windows (Figures 6a and 6b), being detected that the increasing of the persistence for the 6 first moving windows is stabilised for the other 15 windows with notable signs of persistence, with H varying from 0.72 to 0.76. In short, the factor of persistence from the point of view of the Hurst exponent suggests a certain facility of forecasting algorithms, being remarkable that after the first 1000 emissions, (beginning of the five moving window), the highest persistency with some fluctuations is achieved and the highest emissions are included in these windows.

4.2 Embedding dimension.

With respect to the embedding dimension, Figure 7 illustrates five examples of the first segment of 1000 recorded emissions, where the slope, $\mu(m)$, of the $\log_{10}\{C(r)\}$ with respect to $\log_{10}\{r\}$ monotonically increases for an interval of r, being then described the asymptotic evolution of these slopes towards the definitive embedding dimension d_E. The embedding dimensions for the 21 moving windows and the 6 segments are respectively summarised in Table 1 and Table 2. By remembering that this dimension defines the minimum number of non-linear differential equations associated with the physical process, the most complex segments from the mathematical point of view would be the first, second, third and sixth, being not so complex the fourth and fifth ones. Nevertheless, the discrepancies when comparing the different segments are not excessive, given that 9 or 10 differential equations would be sufficient to analyse every one of the 6 segments. A quite different evolution of d_E is obtained for the 21 moving windows (Table 1), with dimensions approximately varying from 9.5 to 6.9. Between the 11th and 13th moving windows d_E diminishes (a more simplified mathematical structure should be assumed for these volcanic emissions) and for the remaining windows (14th -21th) their mathematical structures complexity return to moderate values (7.3 – 7.6).

4.3 The Kolmogorov entropy.

The obtained values of the Kolmogorov entropy exponent, based on equation 6 and summarised in Tables 1 and 2, are also illustrated with some examples (Figure 8). In these four examples, the "loss of memory" of the physical mechanism is quite similar for the 6th segment and the 10th moving window, with values of K which could complicate a bit more the forecasting processes, in comparison with the previous 5th segment and the 13th moving window. In spite of these discrepancies with respect to the "loss of memory" for the different segments and moving windows, they are quite similar in many cases, being only remarkable two examples of extreme minimum (fifth segment, K =0.258) and extreme maximum (10th moving window, K = 0.410). Consequently, the "loss of memory", making complex the forecasting process, would not affect in the same way to all the volcanic explosive emissions.

4.4 The Lyapunov exponents.

A right computation of the Lyapunov exponents needs an iterative process, with the aim of minimising the final uncertainty on every exponent. At the present computations, 975 iterations have been good enough to obtain the first fifteen exponents

190 with very small oscillations at the end of the iterative process. An example of this process is shown in Figure 9, where are described the evolution of the exponents for the third segment of emissions up to λ_{15}. A higher number of exponents is not necessary by two questions. First, the possible errors or uncertainties on forecasting processes could be specially associated with the first Lyapunov exponents. Second, observing the evolution at the end of iterations of the exponents of Figure 9, the Kaplan-Yorke dimension can be computed without the necessity of Lyapunov exponents exceeding dimension 15.

195

The results are summarised in Table 3, showing the mean and standard deviation for every one of the first ten Lyapunov exponents, obtained for the 21 moving windows and the six data segments after 975 iterations of the corresponding computational algorithm to obtain accurate and confident values. First, in agreement with the results exposed in the mentioned table, every one of the λ_i exponents is quite similar both for segments and moving windows, bearing in mind the

200 very similar average values and small standard deviations. Second, the first small negative Lyapunov values are always detected for λ_7 or λ_8. Consequently, the information offered by the Lyapunov exponents, concerning the possible errors on forecasting, should be very similar all along the emissions, being not detected differences between data segments and moving windows. Finally, the Kaplan-Yorke dimension manifests a notable similarity for both, segments and moving window.

205 Whereas for the six trams, D_{KY} varies from 12.51 to 12.75, the range is quite similar for the 21 moving windows, varying from 12.70 to 13.04. Consequently, the fractal dimension of the nucleus around which the consecutive m-dimensional reconstructed vectors describe the corresponding trajectories is complex (a fractal dimension exceeding 12.0). Nevertheless, this complexity becomes confined within a short interval, being quite similar for all segments and moving windows.

210 **5. Some examples of nowcasting**

The nowcasting process (Rundle et al., 2016, 2017) is based on the computation of the "natural time", or in other words, the number of consecutive earthquakes (seismic cycle length) with magnitudes within a determined interval. In this way, the empiric cumulative distribution function, CDF, of these "natural times" would be stablished by the high magnitude earthquakes interrupting these seismic cycle lengths. Consequently, the nowcasting process does not exactly predict a

215 forthcoming high magnitude, but quantify the probability of an imminent high earthquake magnitude, based on the empiric CDFs curves.

A first illustrative example of the nowcasting algorithm, from the point of view of the seismic activity, is depicted in Figure 10a. It corresponds to the recorded seismic activity in Canterbury (National Earthquake Information Database, https://www.gns.cri.nz, years 1990-2020). In spite of the minimum seismic magnitude accomplishing the Gurtenberg-Richter

220 law (Wiemer and Wyss, 2000) should be 3.5 (Figure 10b), maximum magnitudes of 4.5, 5.0 and 5.5, as well as a minimum magnitude of 2.5, have been considered necessaries to obtain a more detailed evolution of the corresponding cycle lengths.

The probability of forthcoming extreme magnitudes (7.2 and 7.8) interrupting a cycle length exceeds 80%. Consequently, the probability of an earthquake of similar extreme magnitudes should be more or less imminent if the real cycling length is approximately ranging between 100 and 1000 "natural times", depending on the chosen maximum magnitude Mmax.

225   Two examples of nowcasting corresponding to volcanic energy explosions are shown in Figure 10b. The first one corresponds to the volcanic activity of the third segment (Figure 2a) and the second includes the whole series of volcanic emissions. In both cases, the cycle lengths are obtained by considering a minimum and maximum level of volcanic emission of, respectively, $10^{2.5}$ J and $10^{4.5}$ J.   Conversely to the example of seismic activity, the few extreme levels exceeding $\log_{10}(Energy) = 8.0$ are not associated with high CDF values. Consequently, the nowcasting algorithm could be considered

230   less effective in comparison with the seismic activity results, probably due to the mechanism of the volcanic emissions, which do not include structures such as background activity, swarms, forecastings, mainshocks and aftershocks. Nevertheless, a notable number of high $\log_{10}(Energy)$ emissions slightly smaller than 8.0, and some of them very close to the highest emissions, are associated with values of CDFs close to 0.6, and even exceeding 0.8. An example of this fact could be the third segment of emissions, where some of them are not independent but associated with the highest emission close to

235   8.5. In short, the nowcasting process could be also assumed as an algorithm contributing to the predictability of volcanic explosions, but perhaps not so obvious as for the case of seismic activities.

6. Discussion of the results

240   The results obtained by the reconstruction theorem and the possible relationships between the fractal reconstructions exponents (H, K, λ and d_E) and changes on the volcanic emissions are summarized in Figures 11a and 11b. First of all, relevant changes on parameters such as mean, standard deviation, skewness and kurtosis (Table 4) are not detected for the different segments of volcanic emissions. Additionally, the Kolmogorov-Smirnov test (95 and 99% of probability) discards the possible Gaussian distribution of these emissions, in agreement with Figures 3a and 3b, where the Generalised logistic

245   distribution (GLO) is assumed from the L-Skewness-Kurtosis formulation.

The Hurst exponent (Figure 11a) is characterised by a continuous increase, finally achieving oscillations close to 0.7, with evident structure of persistence since the 7th up to the 21th moving window, all of them including two high emissions, $\log_{10}(energy) = 8.372$ and 7.937. Consequently, the values of Hurst would manifest persistence (convenient for appropriate forecasting) when a high emission becomes included in the moving window. Conversely, the "loss of memory"

250   (Kolmogorov exponent) of the physical mechanism (not convenient for good forecasting) increases up to the 10th window, notably decreasing for the rest of windows. In this case, the influence of a high emission would appear outdated in comparison with the results of the Hurst exponent. With respect to the Lyapunov exponent, λ_1, its changes along the moving windows are small (Figure 11a) with not very remarkable discrepancies with an average value of 0.169 and a standard deviation of 0.013 (Table 3). Consequently, the different forecasting errors on energy emissions could not be different, at

255   least from the point of view of λ_1. These errors could be also consequence of the degree of complexity of the non-linear

differential equations system, quantified by the embedding dimension, d_E. Figure 11b depicts the clear reduction of this complexity after the 10th moving window, with a fast decrease up to the 13th window and values close to 7.5 after this last cited window. Similar to the evolution of the Kolmogorov entropy, close to the 10th window, an evident decrease of both fractal parameters is detected. Reinforcing this similarity, it is also noticeable the stabilised values of these two fractal

260 parameters for the 13th and 14th windows. It is also convenient to observe that, in agreement with the very similar obtained Kaplan-Yorke dimensions (ranging from 12.5 to 13.0) for segments and moving windows, the data-vectors of high dimension m used for the reconstruction theorem, depict a very similar structure. In other words, the trajectories of these reconstructed vectors around the fractal nucleus are quite similar.

265 With respect to the results of the nowcasting, the return period curves (90%, 95% and 99% of extreme emissions) could be, as cited before, a strategy relatively similar. Nevertheless, the nowcasting process permits to decide minimum and maximum emission of energy levels to define the best empirical distribution of cycle lengths of "natural waiting time", detecting in this way the probability, in percentage, of a probable imminent volcanic emission of high energy. In spite of the nowcasting method does not determine a concrete next volcanic emission, given that it is not a forecasting process, it takes into account

270 that future high emissions will be expected with similar "natural waiting times". Although some emissions, (Figures 10b), exceeding $\log_{10}(Energy) = 7.5$ have probabilities close to 50-60%, probabilities close to or exceeding 80% are also obtained. In short, the nowcasting process seems to be more effective with seismic activity than volcanic emissions. Nevertheless, their results could be also compatible and complementary with algorithms forecasting the high emission of volcanic energy.

275 **7. Conclusions**

The fractal parameters, obtained by means of the reconstruction theorem of 6 segments and 21 moving windows of the analysed volcanic explosions in Volcán de Colima (México), as well as the nowcasting strategy, are the first steps for the application of different forecasting processes.

The results suggest that different strategies for future forecasting emissions can be applied, especially for high-energy

280 emissions. These forecasting strategies can be based on different algorithms (Box and Jenkins, 1976; Lipton et al, 2015; Rundel et al., 2017 and Lei, 2021, among others) and multifractal analysis of moving window data (Monterrubio-Velasco et al., 2020). In spite of the uncertainties with respect to the waiting time of an emission and its corresponding energy, estimated by means of forecasting, are expected to be non-negligible, these algorithms should depict reasonably good approaches to real energy emissions bearing in mind the obtained reconstruction theory results. Additionally, the analysis of

285 the multifractal structure is expected to be a warning factor for volcanic activities associated with high emissions of energy, quite similar to the analysis of consecutive seismic magnitudes (Monterrubio-Velasco et al., 2020) and usefully applied to analyse climatic data, thermometric and pluviometric data, (Burgueño et al., 2014; Lana et al., 2023) and also bearing in mind (Shimizu et al., 2002) the concept of multifractal complexity index, which could also contribute to detect imminent extreme volcanic emissions of energy. In short, the reconstruction theory applied in this research, together with nowcasting

290 and forecasting algorithms and multifractal theory could be a very important process to prevent extreme emissions of volcanic energy. .

Competing interests

The contact author has declared that none of the authors has any competing interests

295

Acknowledgments

The research leading to these results has received funding from the European High-Performance Computing Joint Undertaking (JU) and Spain, Italy, Iceland, Germany, Norway, France, Finland, and Croatia, under grant agreement No. 101093038, ChEESE-CoE

300

Data availability

Data sharing is not applicable to this article as no new data were created or analyzed in this study.

References

Arámbula-Mendoza, R., Reyes-Dávila, G., Vargas-Bracamontes, D. M., González-Amezcua M., Navarro-Ochoa, C.,
305 Martínez-Fierros, A., Ramírez-Vázquez, A. Ariel: Seismic monitoring of effusive-explosive activity and large lava dome collapses during 2013–2015 at Volcán de Colima, Mexico, J. Volcanol. Geotherm. Res., 351, 75-88, doi:10.1016/j.jvolgeores.2017.12.017, 2018.

Arámbula-Mendoza, R., Reyes-Dávila, G., Domínguez-Reyes, T., Vargas-Bracamontes, D., González-Amezcua, M.,
310 Martínez-Fierros, A., Ramírez-Vázquez, A: Seismic Activity Associated with Volcán de Colima. In Volcán de Colima, portrait of a Persistently Hazardous Volcan, doi:10.1007/978-3-642-25911-1_1, Ed. Springer, 2019.

Bachtell Clarke, A., Esposti Ongaro, Belousov T.: Vulcanian eruptions. The Encyclopedia of Volcanoes, Editor in chief, Haraldur Sigurdsson. Elsevier.
315
Box, G.E.P. and Jenkins, G.M. (1976) Time Series Analysis: Forecasting and Control. CA: Holden-Day 575 pp., doi:10.1016/B978-0-12-385938-9.00028-6, 2015.

Burgueño, A. Lana, X., Serra, C., Martínez, M.D. (2014). Daily extreme temperature multifractals in Catalonia (NE Spain).
320 Physical Letters A, 378, 874-885.

Diks, C.: Nonlinear time series analysis. Nonlinear Time Series and Chaos, vol. 4. World Scientific Edit., 209 pp. Doi: 10.1017/CBO9780511755798, 1999.

325 Eckmann JP, Oliffson S, Ruelle D, Cilliberto S.: Lyapunov exponents from time series, Phys. Rev. A., 34(6): 4971–4979, doi: 10.1103/PhysRevA.34.4971, 1986.

Grassberger P, Procaccia I.: Characterization of strange attractors. Physical Review Letters, 50, 346–349, 1983a.

330 Grassberger P, Procaccia I.: Estimation of the Kolmogorov entropy from a chaotic signal. Physical Review A, 28, 448–451, 1983b.

Gutenberg B, Richter C.: Frequency of earthquakes in California. Bull Seismol Soc Am 34:185–188, 1944.

335 Hosking, J.R.M., Wallis, J.R.: Regional frequency analysis. An approach based on L-moments. Cambridge University Press, 224 pp, 1997.

Kantelhardt JW, Zschiegner SA, Koscielny-Bunde E, Havlin S, Bunde A, Stanley HE.: Multifractal detrended fluctuaction analysis of nonstationary time series. *Physica A, 316*, 87–114, 2002.

340

Kaplan JK, Yorke JA.: Chaotic behaviour of multidimensional difference equations. In *Functional Difference Equations and Approximation of Fixed Points*, Vol. 730, Walter HO, Peitgen HO (eds). Springer Verlag: Berlin, 204–227, 1979.

Lana, X., Rodríguez-Solà, R., Martínez, M.D., Casas-Castillo, M.C., Serra, C. and Kichner, R.: Autoregressive process of
345 monthly rainfall amounts in Catalonia (NE Spain) and improvements on predictability of length and intensity of drought episodes. International Journal of climatology, 41, 3178-3194. doi.org/10.1002/joc.6915., 2021.

Lana, X., Casas-Castillo, M.C., Rodríguez-Solà, R., Prohoms, M., Serra, C., Martínez, M.D., Kirchner, R. (2023). Time trends, irregularity, multifractal structure and effects of CO_2 emissions on the monthly rainfall regime at Barcelona city, NE
350 Spain, years 1786-2019. International Journal of Climatology. https://doi.org/10.1002/joc.7786.

Lei, C.: RNN, Deep Learning and Practice with MindSpore. Springer Singapore, pp 83-93, 2021.

355 Lipton, Z.C, Berkowitz, J., Elkan, C.: A critical review of recurrent neural networks for sequence learning. arXiv preprint arXiv:1506.00019, 2015.

Monterrubio-Velasco, M., Lana, X., Martínez, M.D. Zúñiga, R. and de la Puente, J.: Evolution of the multifractal parameters along different steps of a seismic activity. The example of Canterbury 2000-2018 (New Zealand). American Institute of
360 Physics. AIP Advances. Doi: 10.1063/5.0010103, 2020.

Rundle, J.B., Turcotte, D.L., Donnellan, A., Grant, Ludwig, L., Luginbuhl, M., Gong, G.: Nowcasting earthquakes. AGU Publications. https://doi.org/10.1002/2016EA000185, 2016.

365   Rundle, J.B., Luginbuhl, M., Giguere, A., Turcotte, D.L.: Natural time, nowcasting and the physics of earthquakes: estimation of seismic risk to global megacities. Pure and Applied Geophysics. DOI 10.1007/s00024-017-1720-x, 2017.

Stoop F, Meier PF.: Evaluation of Lyapunov exponents and scaling functions from time series. *J. Opt. Soc. Am. B*5: 1037–
370   1045, 19898

Turcotte DL.: Fractals and Chaos in Geology and Geophysics, 2nd edition. Cambridge University Press. Cambridge, UK, 398 pp, 1997.

375   Wiemer, S. and Wyss, M. (2000) Minimum Magnitude of Completeness in Earthquake Catalogs: Examples from Alaska, the Western United States, and Japan. Bulletin of the Seismological Society of America, 90, 859-869. https://doi.org/10.1785/0119990114

380   Wiggins S.: Introduction to Applied Nonlinear Dynamical Systems and Chaos. Text in Applied Mathematics, Vol. **2**, 2nd edn. Springer, New York, NY, 843 pp, 2003.

385

390

395

Table 1. Embedding dimension and Kolmogorov coefficient for the 21 moving windows.

MW	1	2	3	4	5	6	7	8	9	10	11
d_E	9.356	9.309	9.195	9.037	9.287	9.237	9.246	9.044	9.361	9.456	8.898
K	0.362	0.363	0.355	0.357	0.354	0.362	0.383	0.373	0.391	0.410	0.397

MW	12	13	14	15	16	17	18	19	20	21
d_E	7.188	6.910	7.277	7.270	7.372	7.385	7.495	7.550	7.467	7.495
K	0.297	0.266	0.279	0.286	0.281	0.284	0.295	0.297	0.291	0.287

400

Table 2. Embedding dimension and Kolmogorov coefficient for the 6 segments of volcanic emissions.

SEGMENT	1	2	3	4	5	6
d_E	9.155	8.932	8.727	7.952	8.101	9.340
K	0.359	0.338	0.377	0.375	0.258	0.398

405 **Table 3**. Mean and standard deviation for the first ten Lyapunov exponents, after 975 iterations.

SEGMENT	$\lambda 1$	$\lambda 2$	$\lambda 3$	$\lambda 4$	$\lambda 5$	$\lambda 6$	$\lambda 7$	$\lambda 8$	$\lambda 9$	$\lambda 10$
$<\lambda>$	0.156	0.105	0.074	0.053	0.032	0.015	-0.001	-0.018	-0.039	-0.062
$\sigma(\lambda)$	0.011	0.004	0.005	0.004	0.003	0.003	0.004	0.005	0.003	0.004

Table 4. Basic characteristics of the energy emissions (logarithm of energy), for the whole database, the 6 segments of 1,000 elements and the last segment of 182 elements. The empirical results of the Kolmogorov-Smirnov, K-S, test are compared with the significance levels of 95 and 99%, KS_0.05 and KS_0.01, corresponding to the Gaussian distribution.

SEGMENT	0001-6182	0001-1000	1001-2000	2001-3000	3001-4000	4001-5000	5001-6000	6001-6182
MAXIMUM	8.903	8.187	7.574	8.372	7.937	7.650	7.667	8.903
MEAN	6.610	6.578	6.563	6.641	6.663	6.558	6.633	6.730
ST.DEV	0.283	0.233	0.225	0.313	0.310	0.242	0.292	0.470
SKEWNESS	1.394	1.252	0.931	1.267	1.035	1.144	0.834	2.085
KURTOSIS	3.462	3.695	0.780	2.033	1.016	1.328	0.110	5.394
K-S TEST	0.102	0.081	0.083	0.106	0.091	0.102	0.095	0.154
K-S_0.05	0.017	0.043	0.043	0.043	0.043	0.043	0.043	0.100
K-S_0.01	0.021	0.051	0.051	0.051	0.051	0.051	0.051	0.120
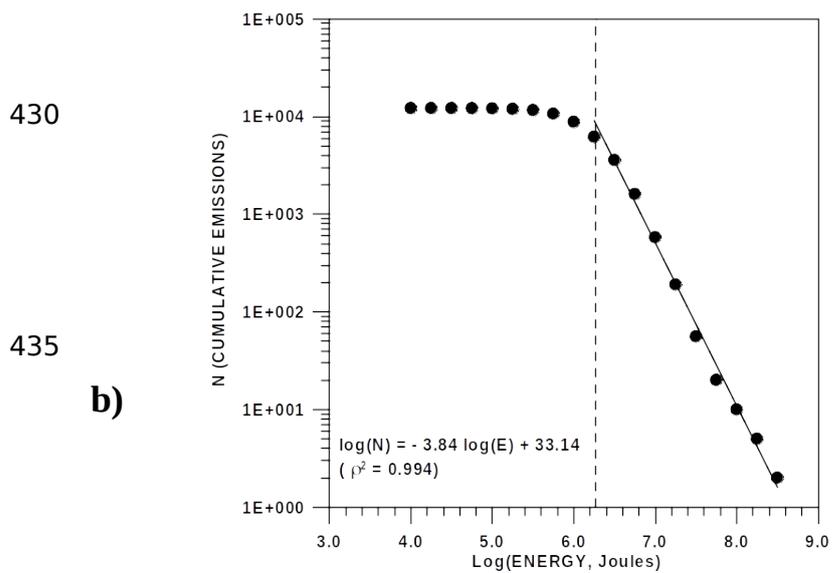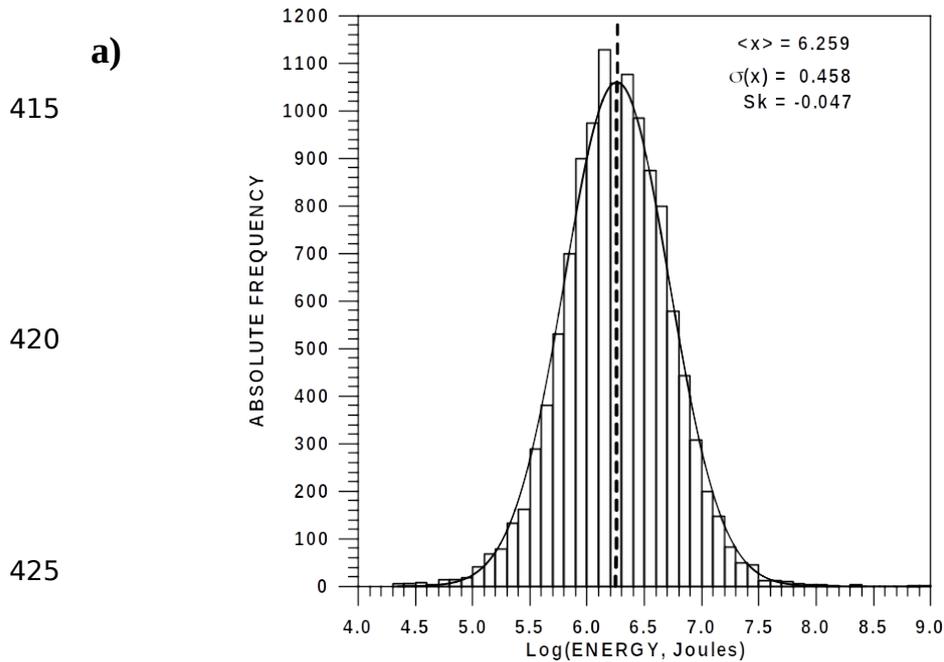
410

Figure 1. a) Histogram of the volcanic emission energies and b) logarithm of energies accomplishing the Gutenberg-Richter law.

445

450

455

460

465

470
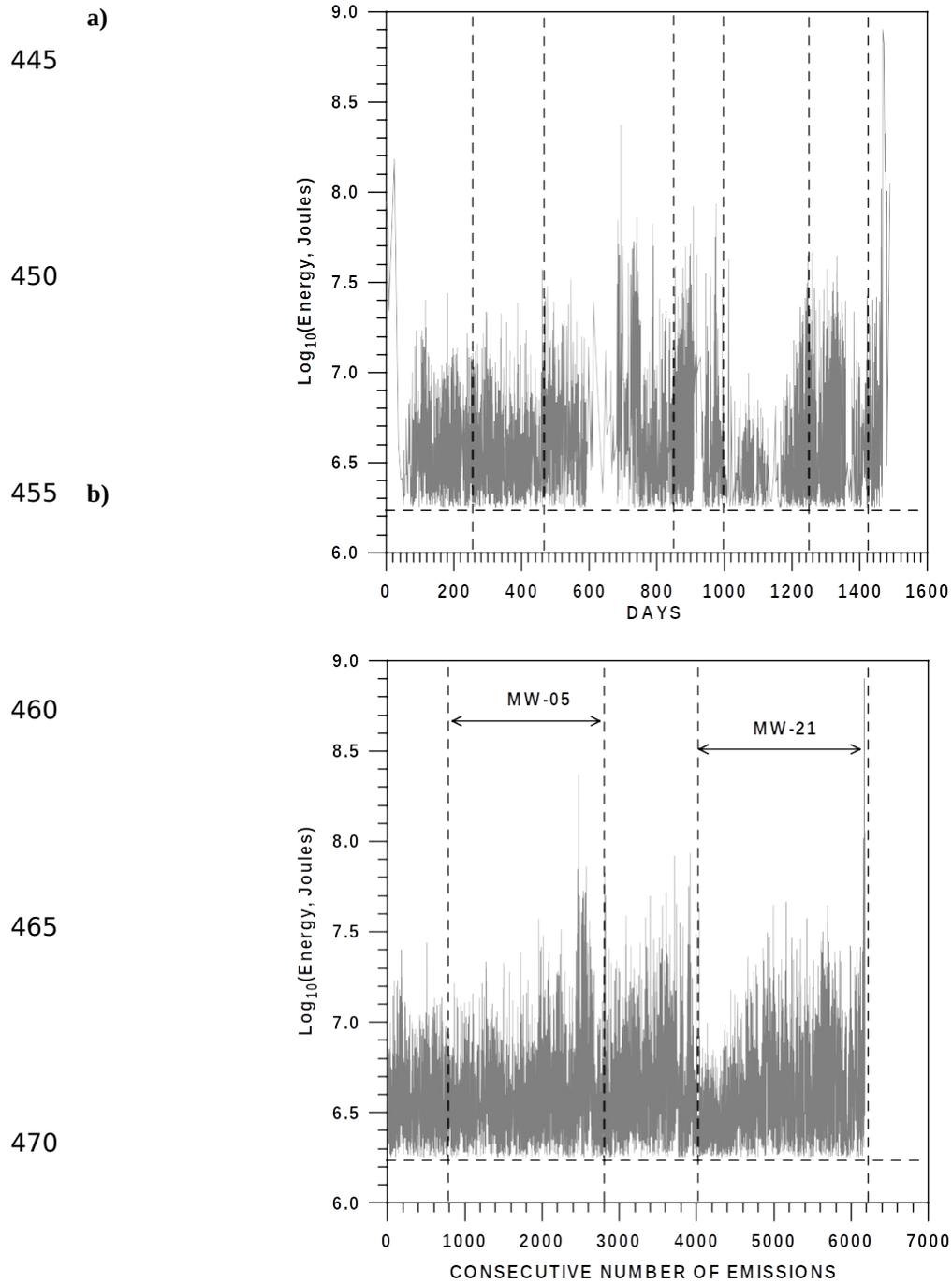
Figure 2. a) Evolution of the volcanic energy emission accomplishing the Gutenberg-Richter law. Vertical dashed lines

475   define the segments (intervals of 1000 data) b) Two examples of dataset defined by moving windows of amplitude 2

thousand elements and shift of 200 positions.
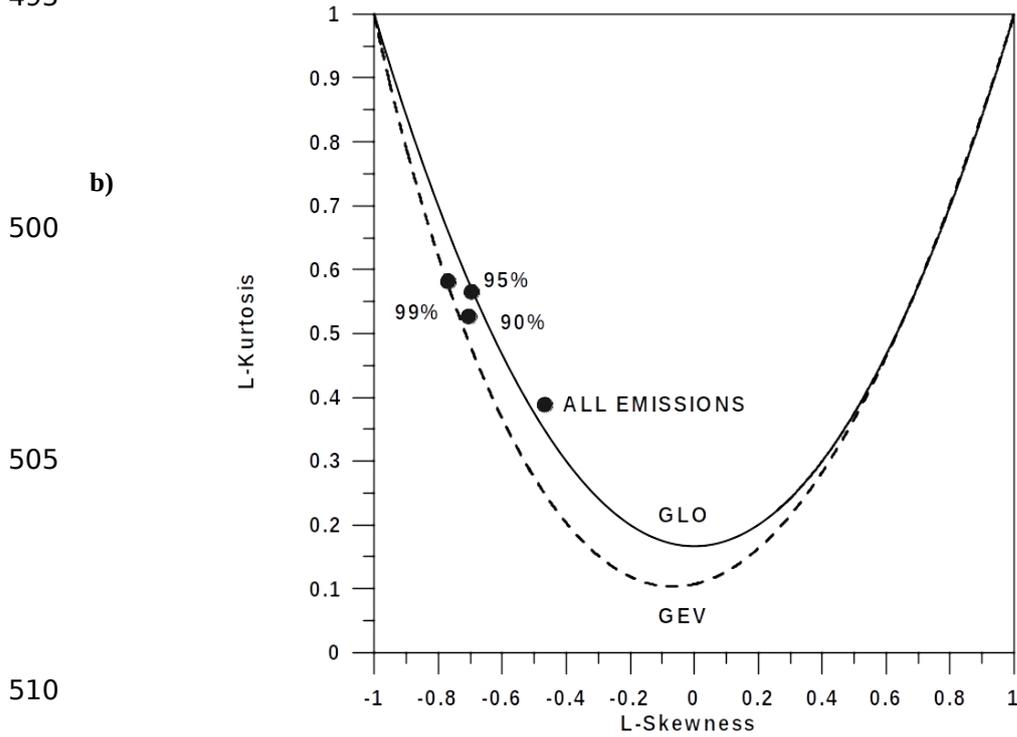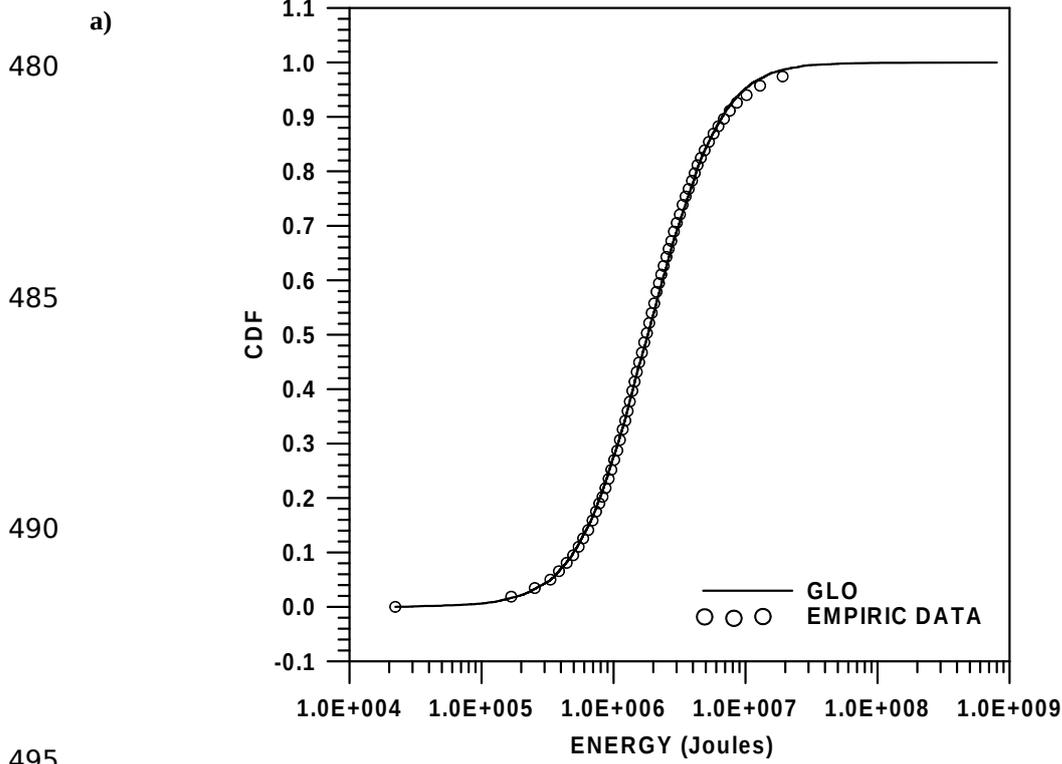
Figure 3. a) Cumulated distribution function of the effusive volcanic energy emissions, well fitted to the GLO (generalised logistic distribution). b) The emissions equalling to or exceeding 90%, 95% and 99% could be associated with the GEV (generalised extreme values distribution) in agreement with the L-Skewness / L-Kurtosis diagram. The theoretical cumulated distribution GLO of the volcanic emissions is also confirmed by means of the mentioned diagram.

515

520

525

530

535

540

545
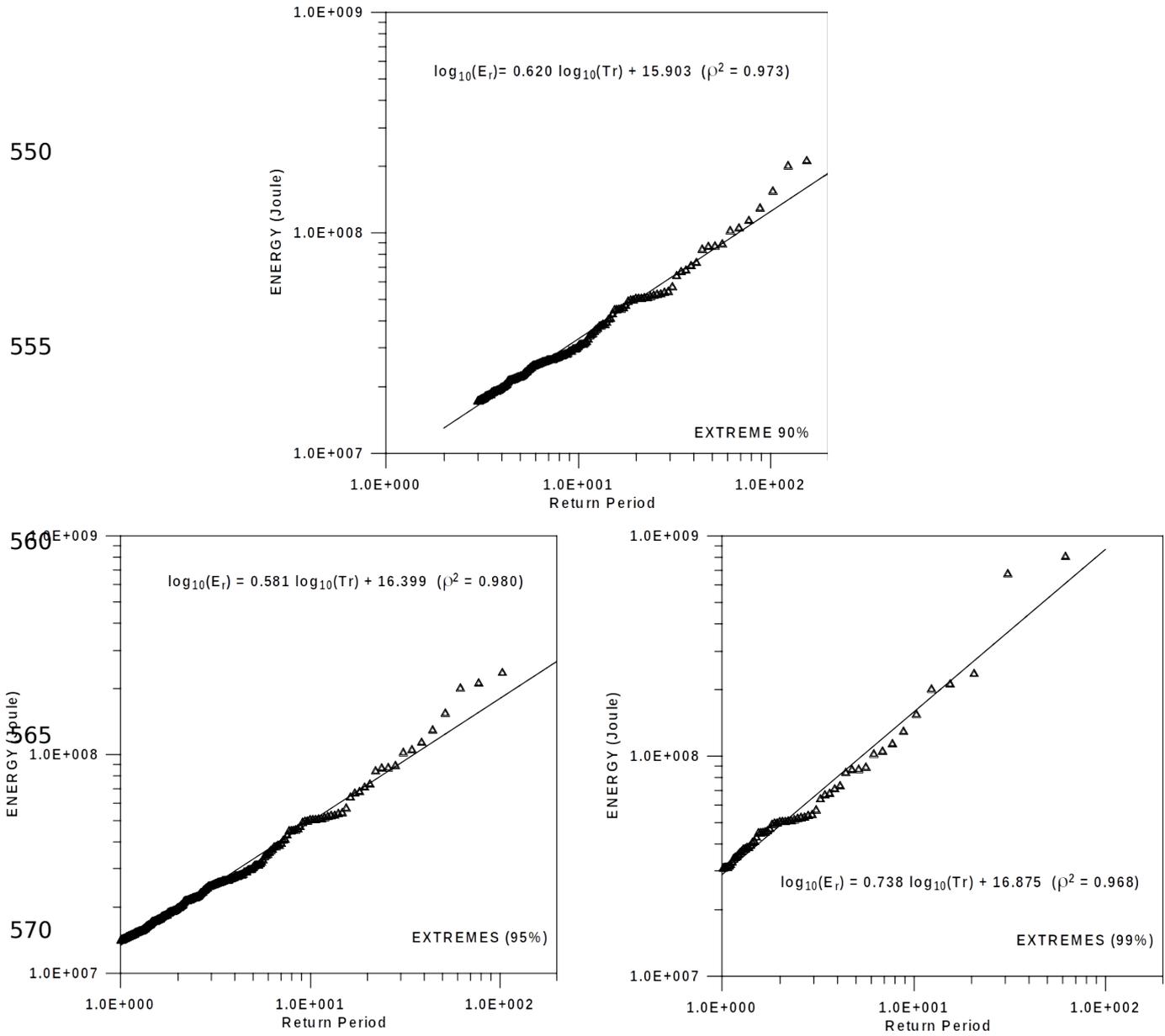
Figure 4. Return period curves (90, 95 and 99%) of extreme emissions.

550

555

560

565

570

575

580

a)

585

590

b)

595

610

615
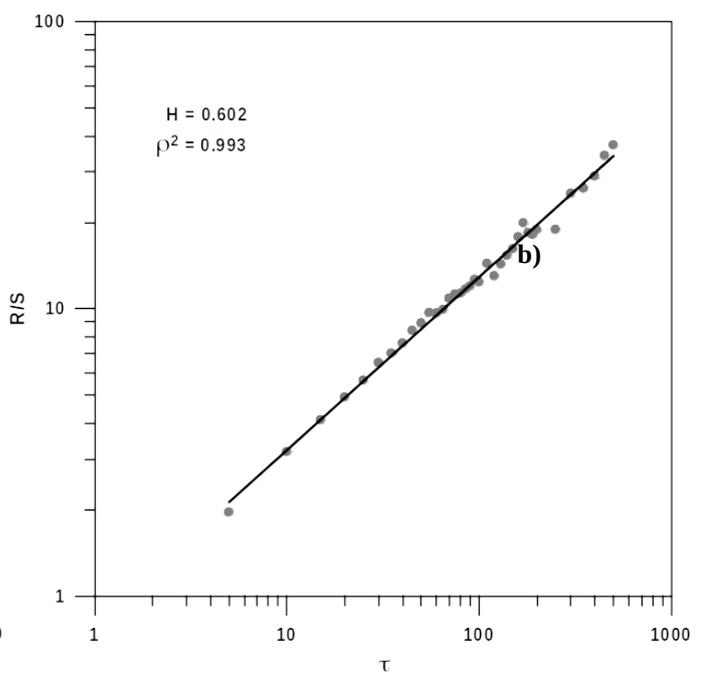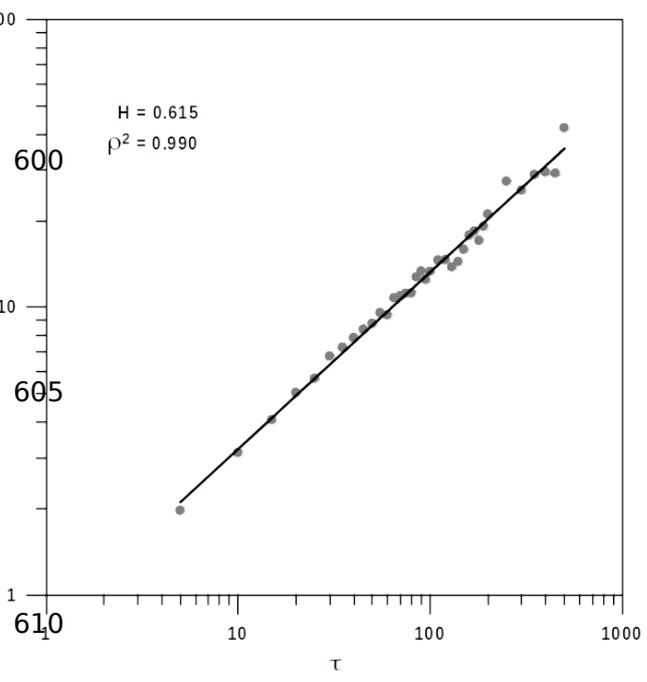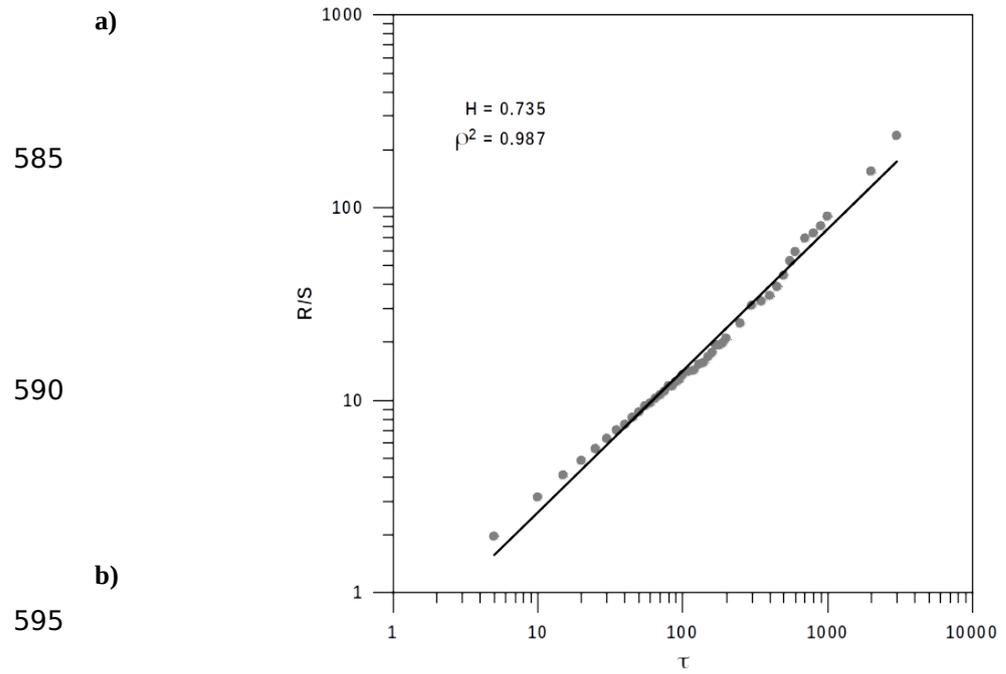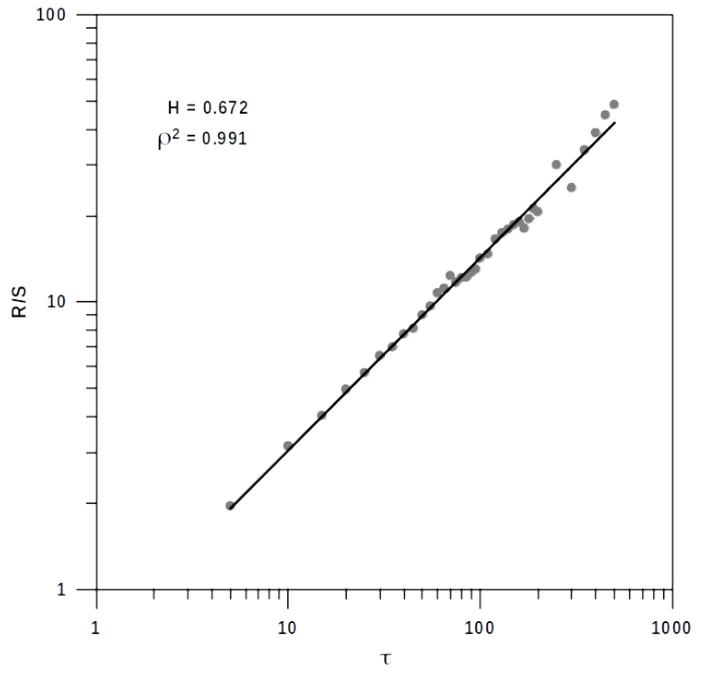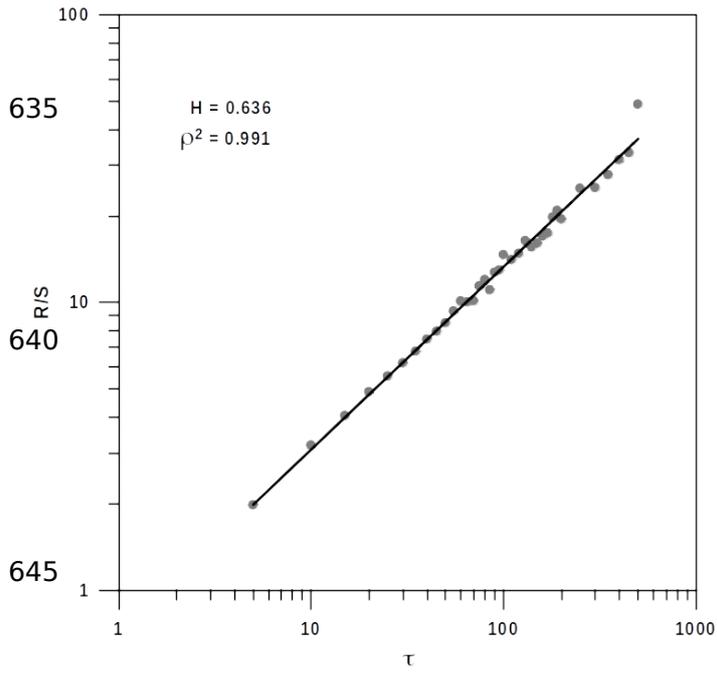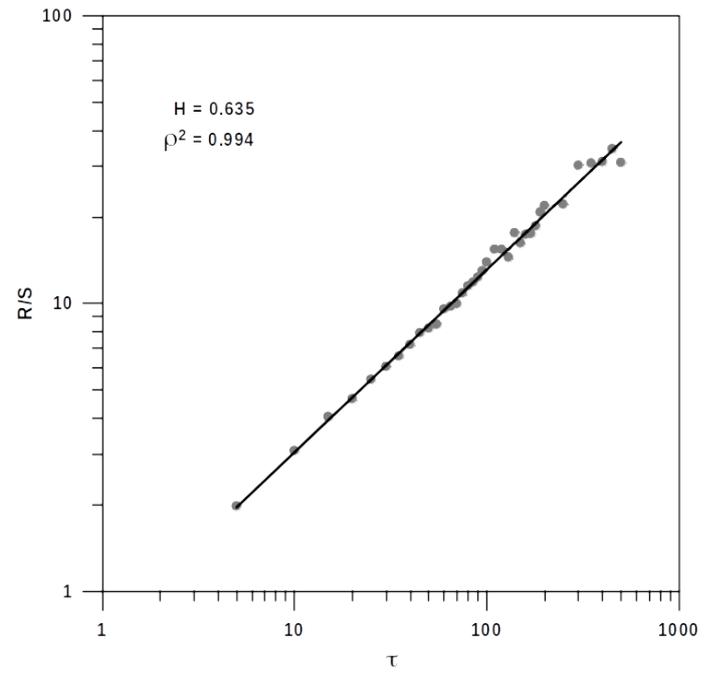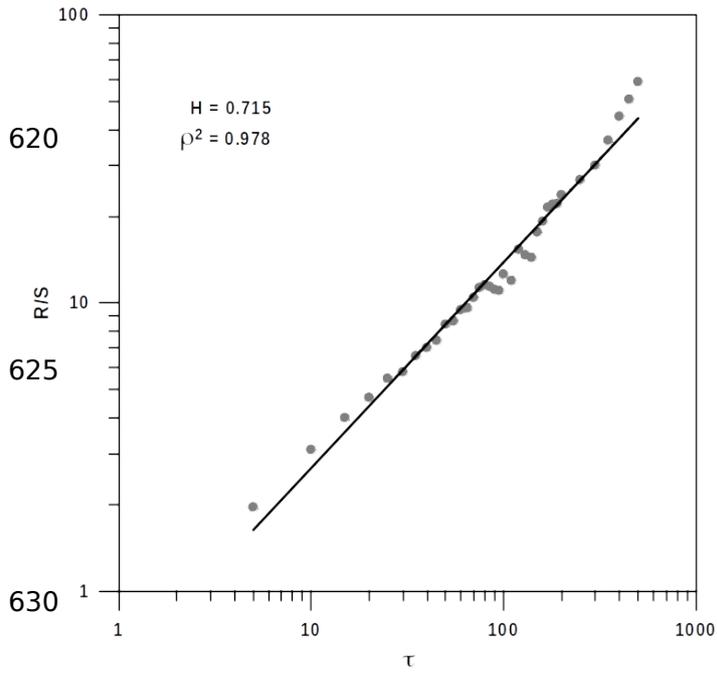
Figure 5. Some examples of the Hurst exponent for a) the whole series of effusive emissions of energy accomplishing the Gutenberg-Richter law and b) the same series fragmented on six trams of equal number of records. In agreement with the definition of equation (1), R/S has not units and ⤭ represents the different lengths (number of data) of the segments considered.

655

660

665

670

675

680
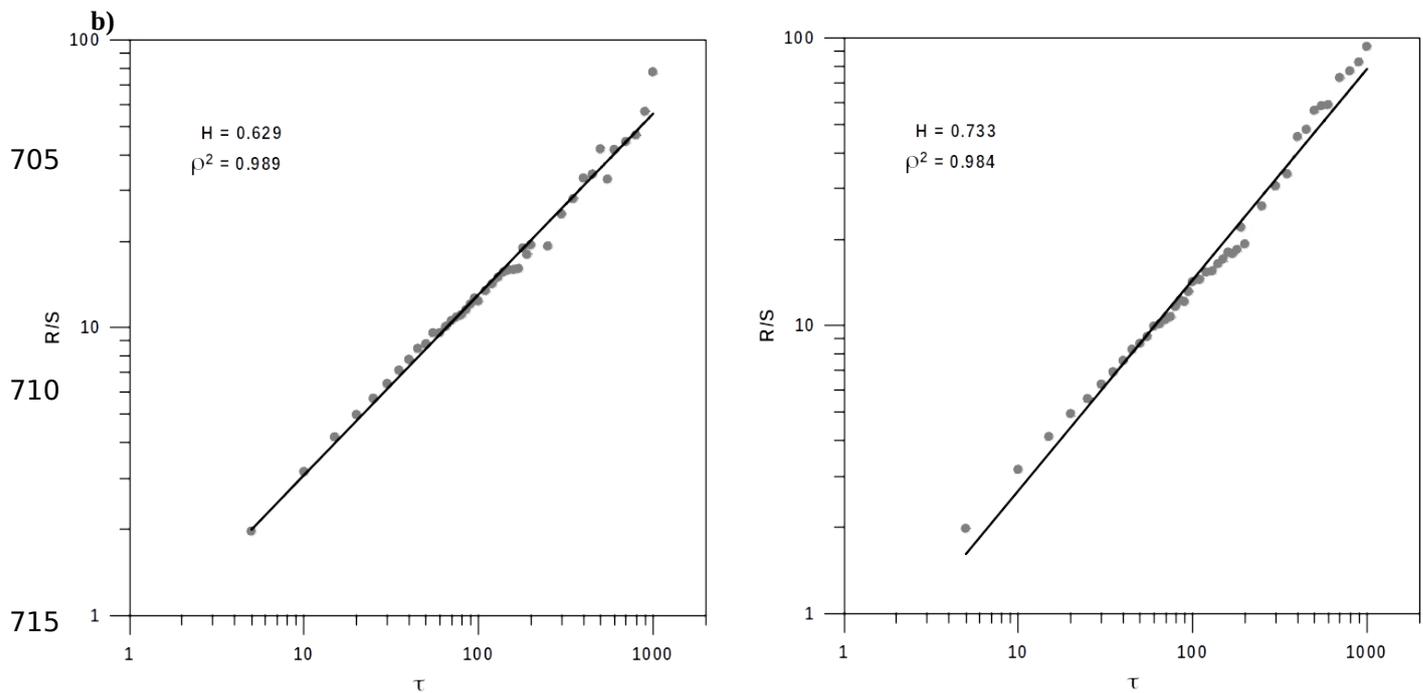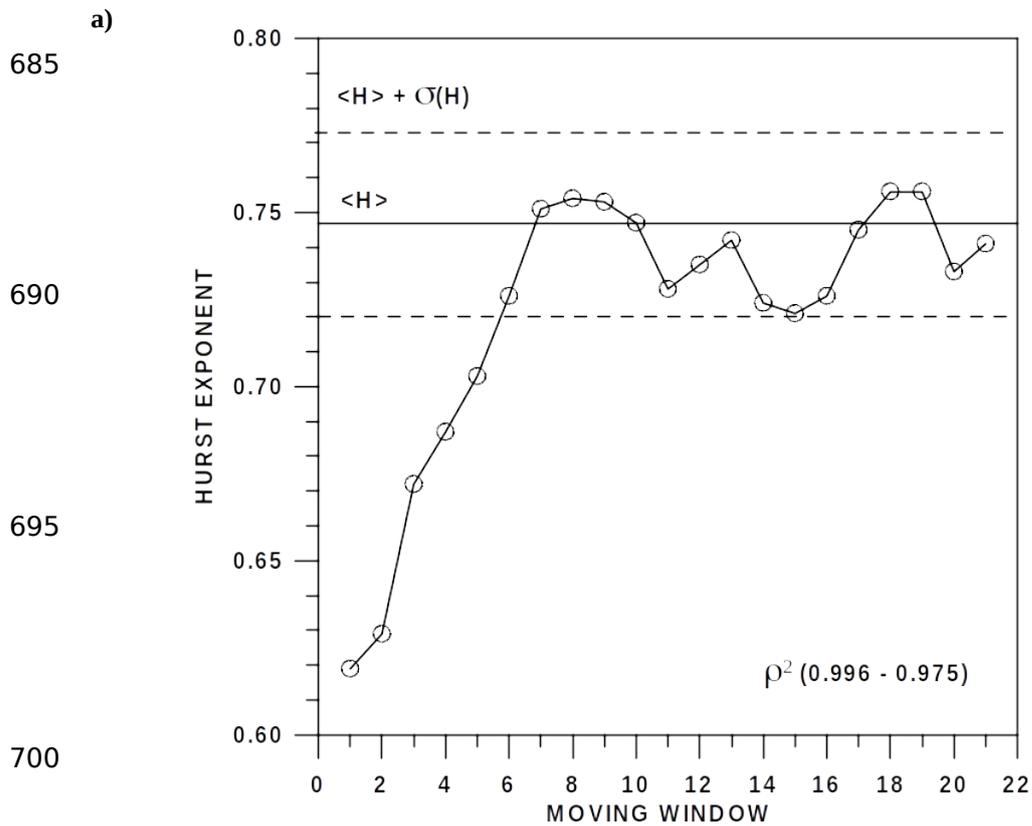
Figure 6. a) Evolution of the Hurst exponent for the 21 moving windows and b) two examples for windows 2 and 6.

720

725

730

735

740

745

750

755

760

765

770
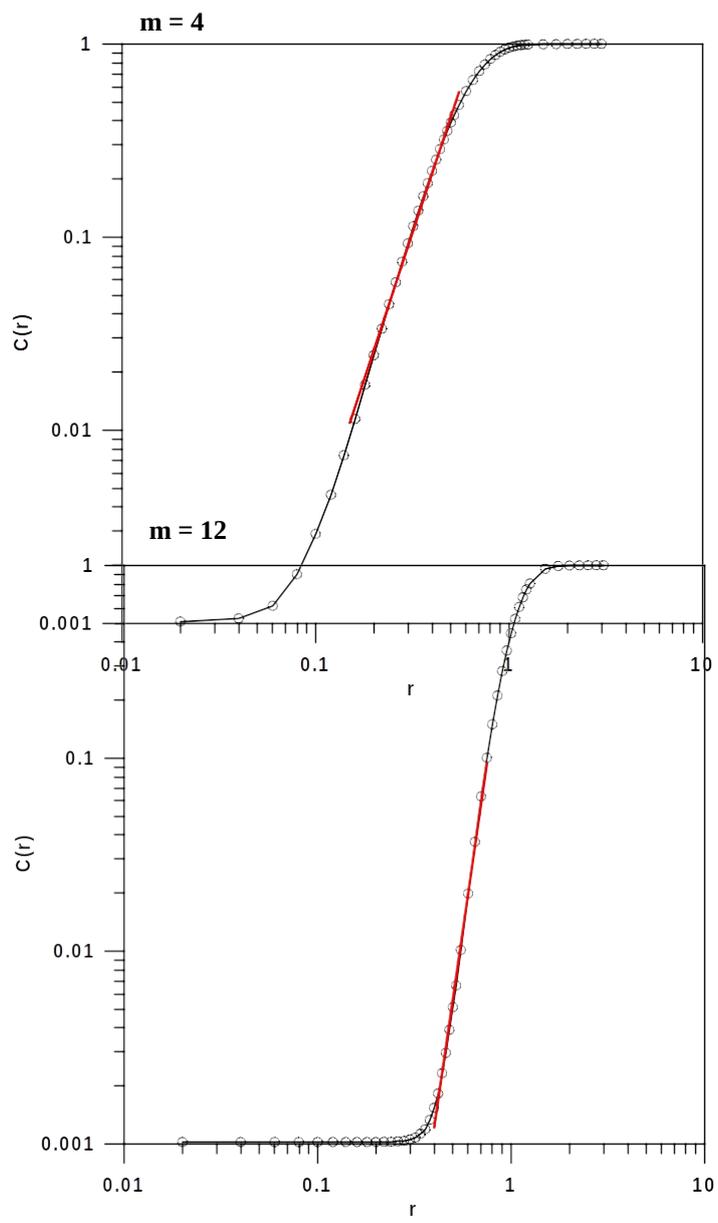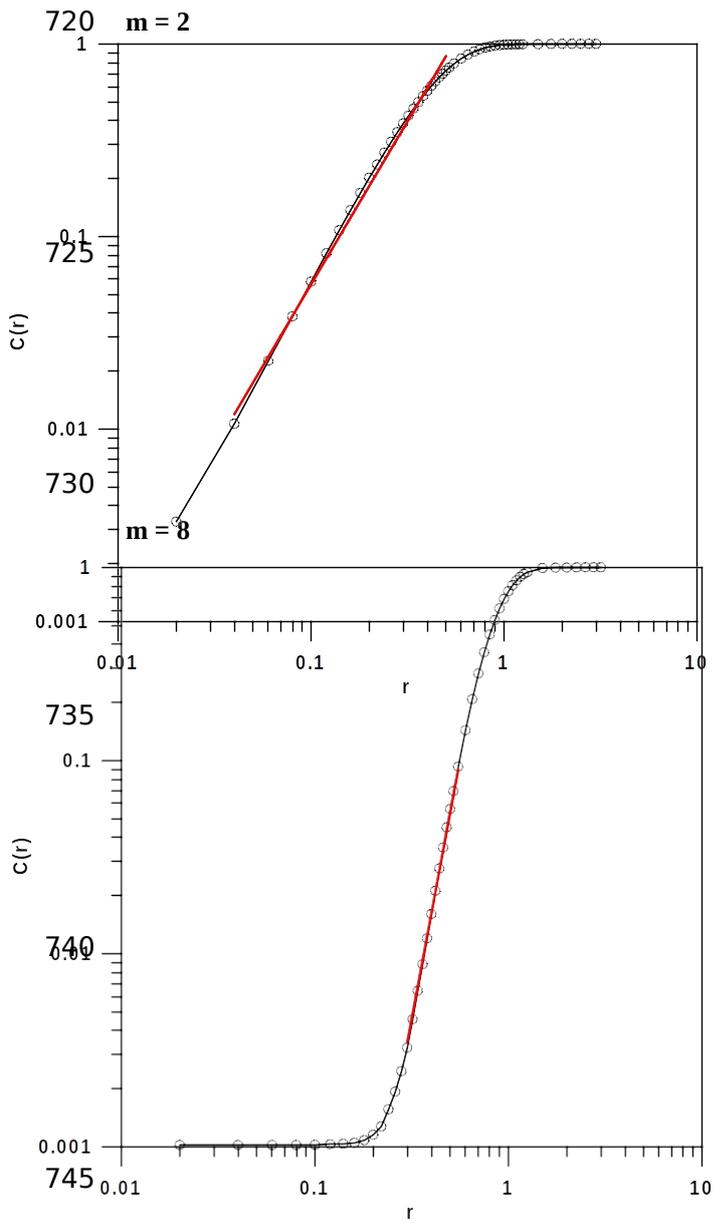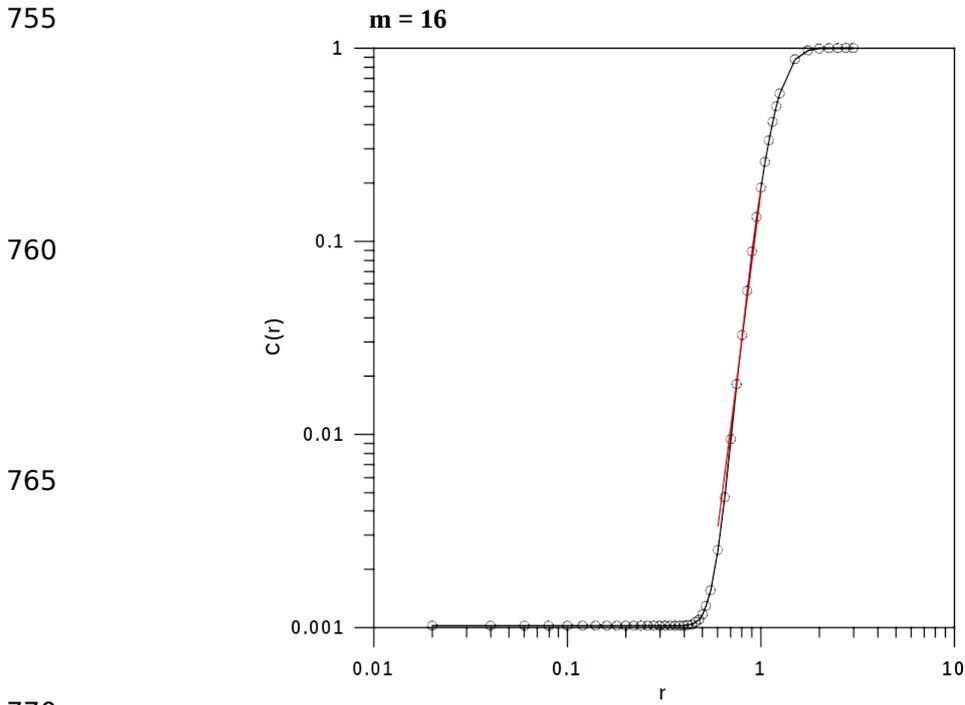
Figure 7. An example of the evolution of embedding dimension (first segment of 1000 elements) for reconstruction dimensions m = 2, 4, 8, 12, 16. The straight red line represents the interval of r values for which can be determined every one of the embedding dimensions.

775

780

785

a)
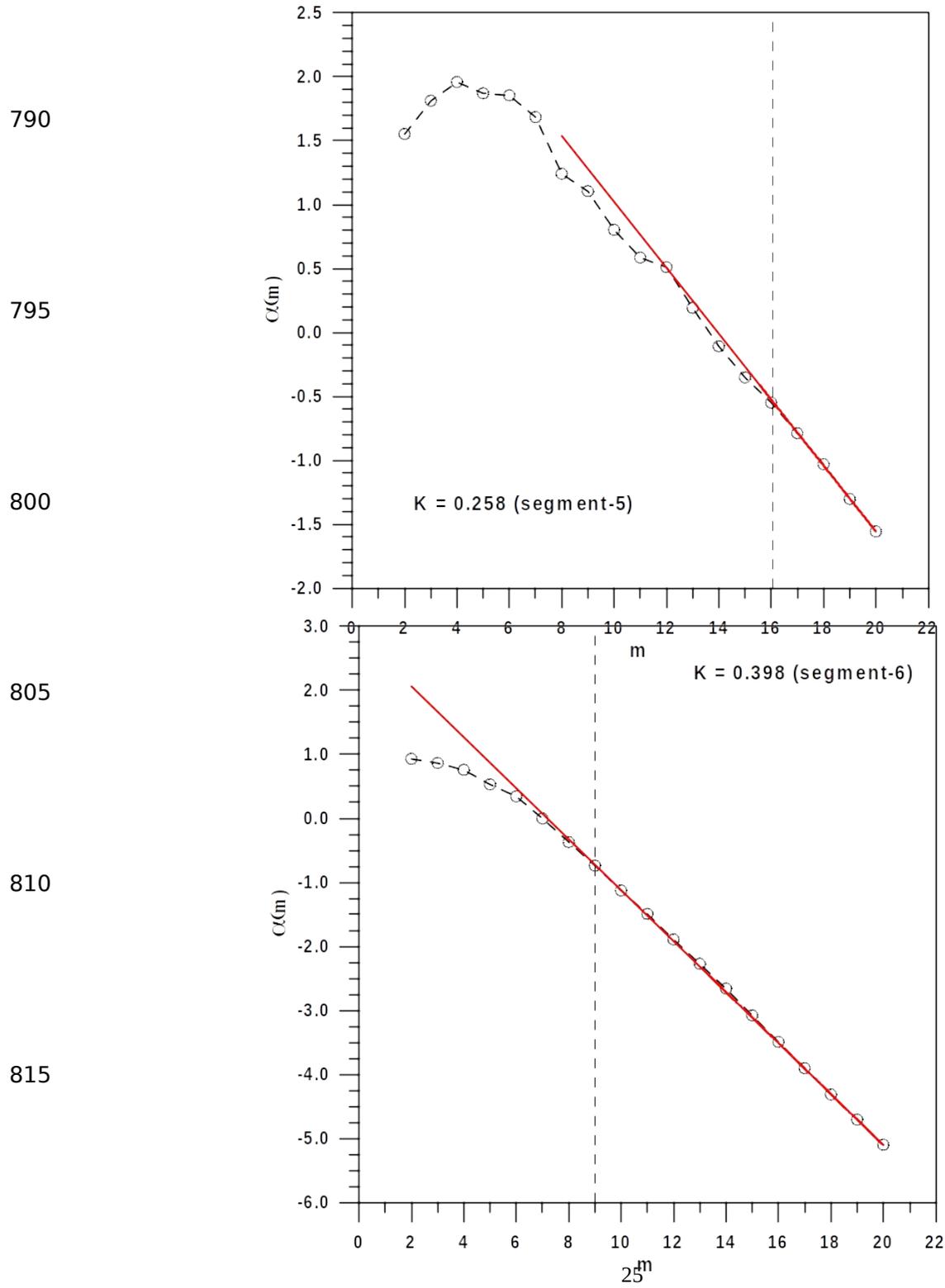
820 **(Figure 8 continue)**
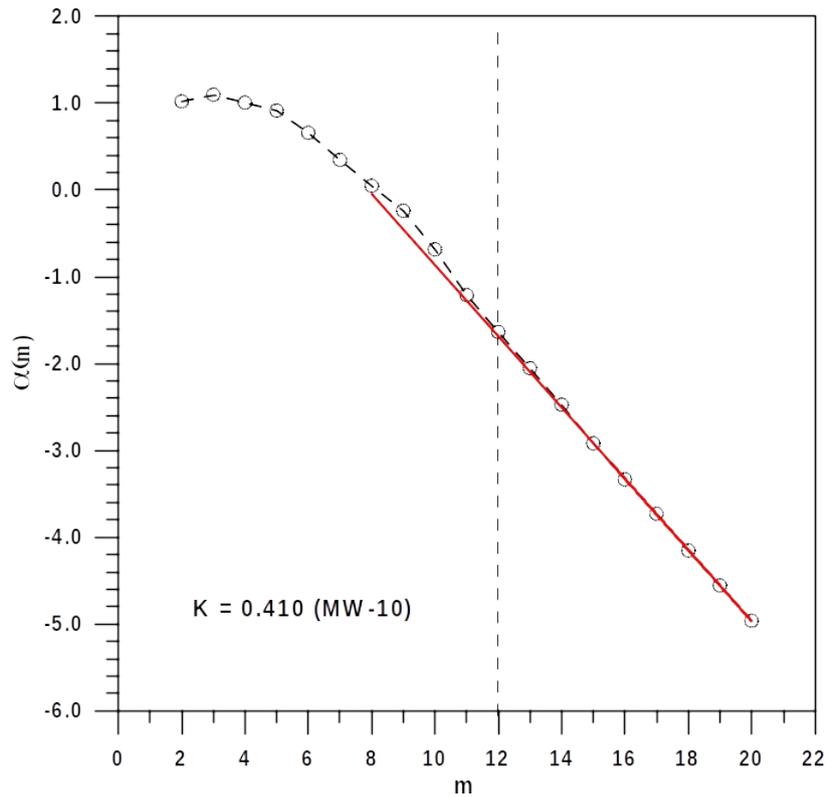
(b)
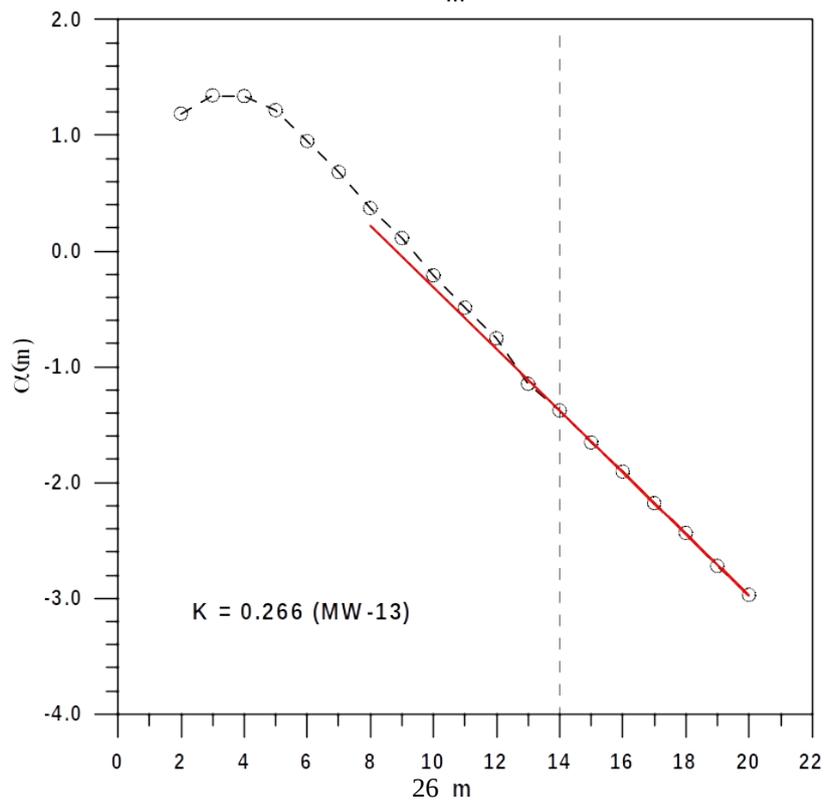
855 **Figure 8**. a) Two examples of Kolmogorov entropy exponents, K, for two segments of 1000 elements and b) for two
examples for moving windows. The vertical dashed lines define the parameter m interval used to determine the Kolmogorv
entropy for every data segment or moving window.

860

865

870

875

880

885
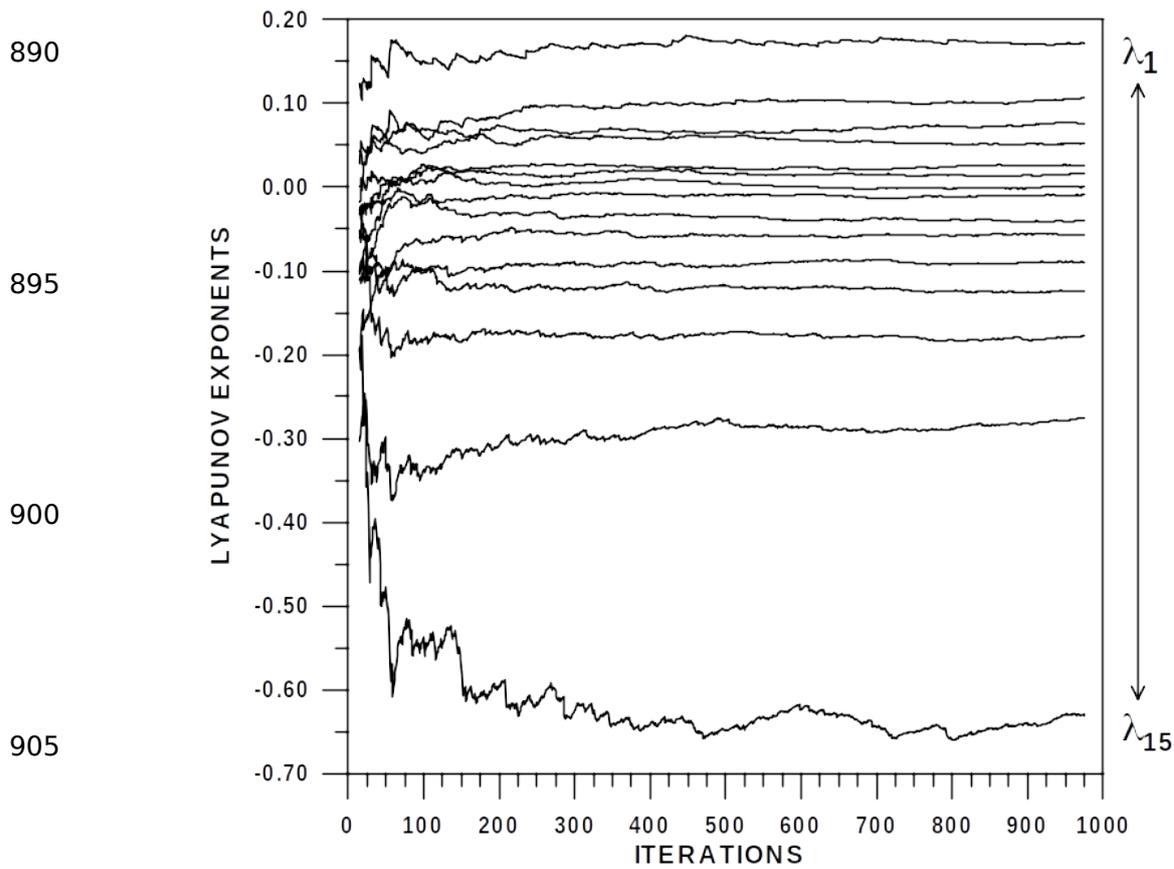
Figure 9. Fifteen Lyapunov exponents for the third segment of the effusive-explosive volcanic emissions.

a)

b)

rr

960

965

970
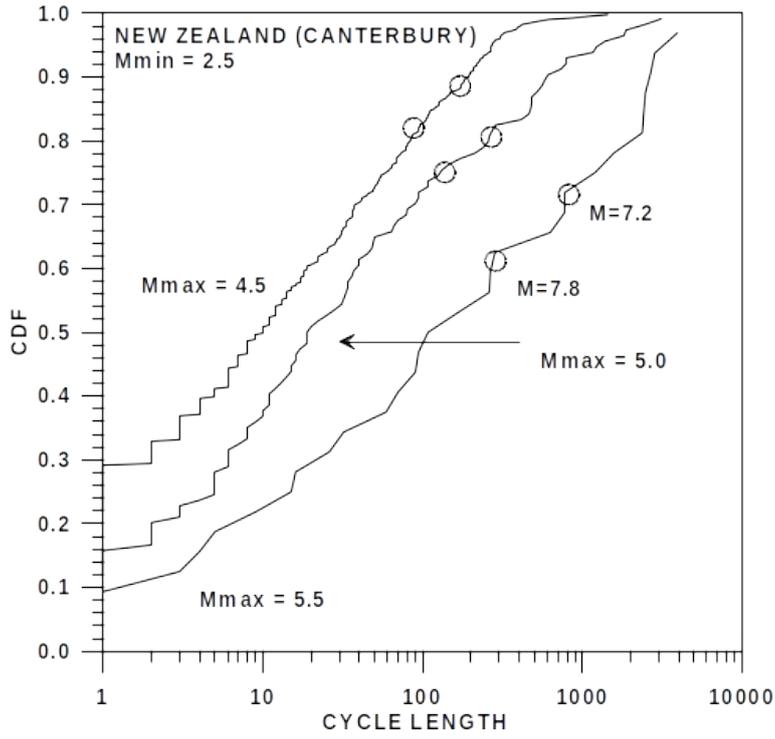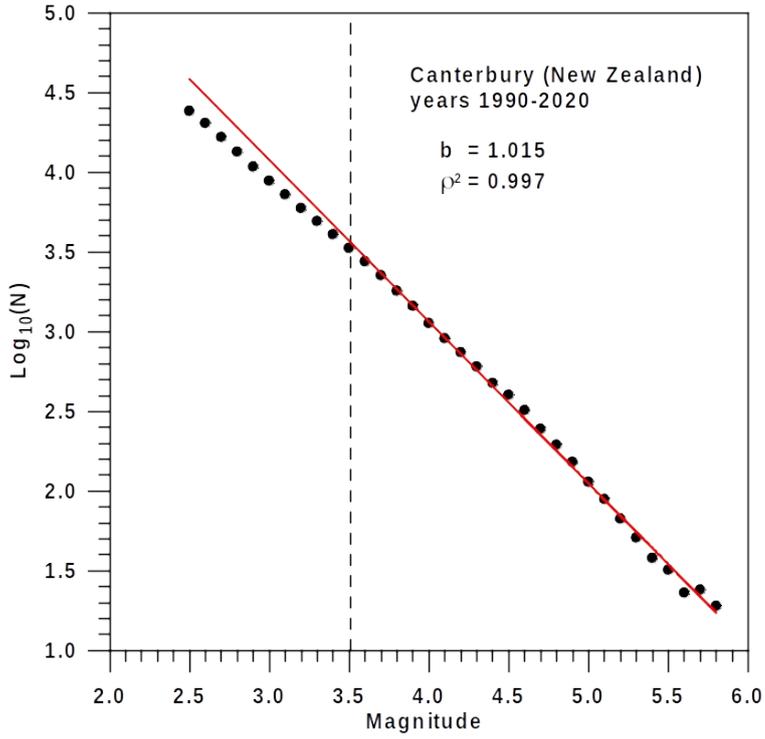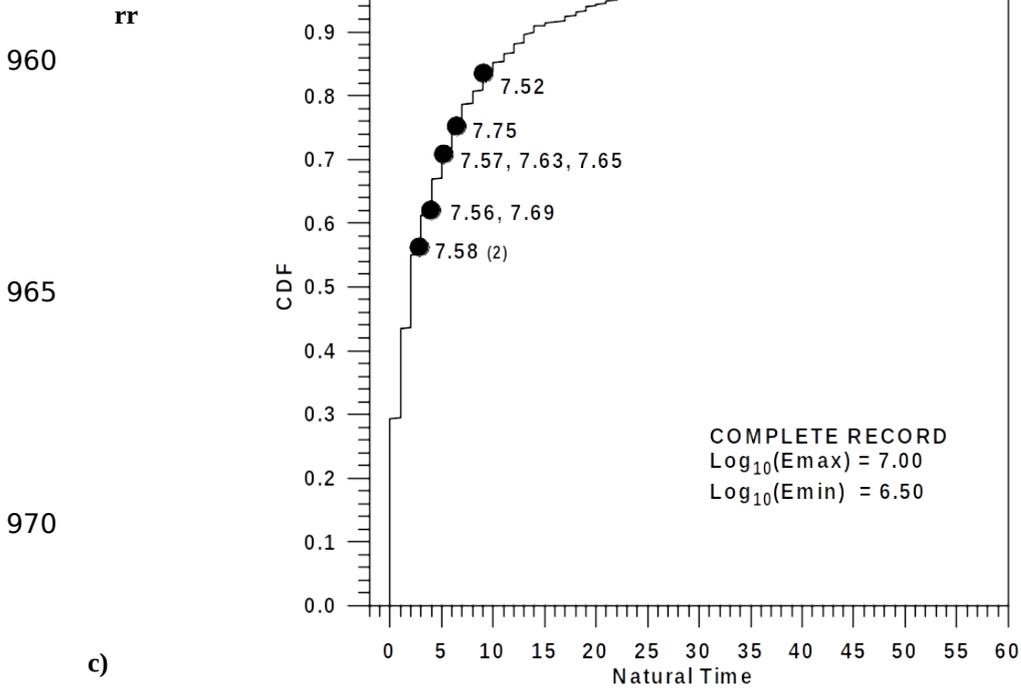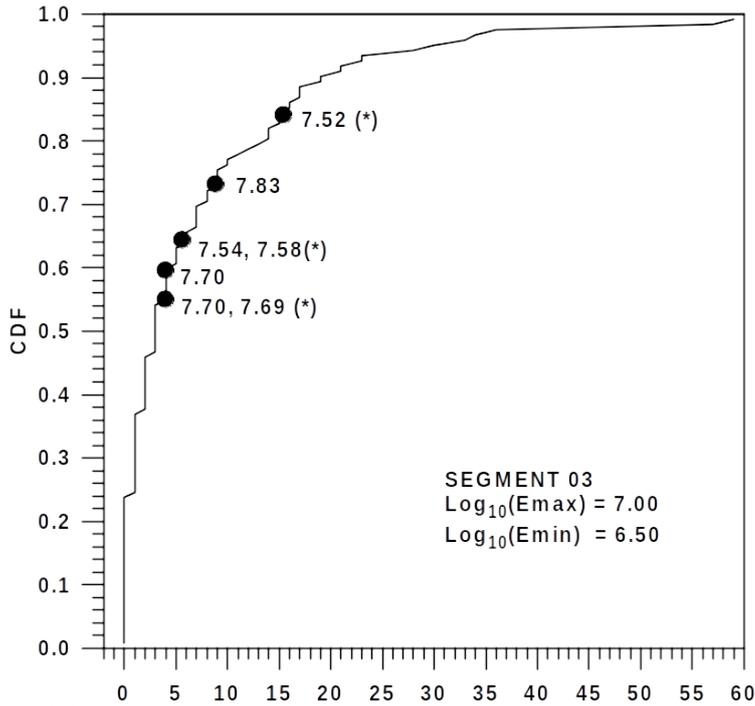
c)

975 **Figure 10.** A comparison of nowcasting results for a) the seismic activity of Canterbury (New Zealand), years 1990-2021, and b) the corresponding Gutenberg-Richter plot and c) the energy of the volcanic emissions of Colima (México), years 2013-2015, bearing in mind the SEGMENT 03 of volcanic emissions and all the volcanic record. The extreme three volcanic records designed by an asterisk (Figure 10b) are the same detected in the Figure 10c.

980

985

990

995

1000

1005

1010

a)
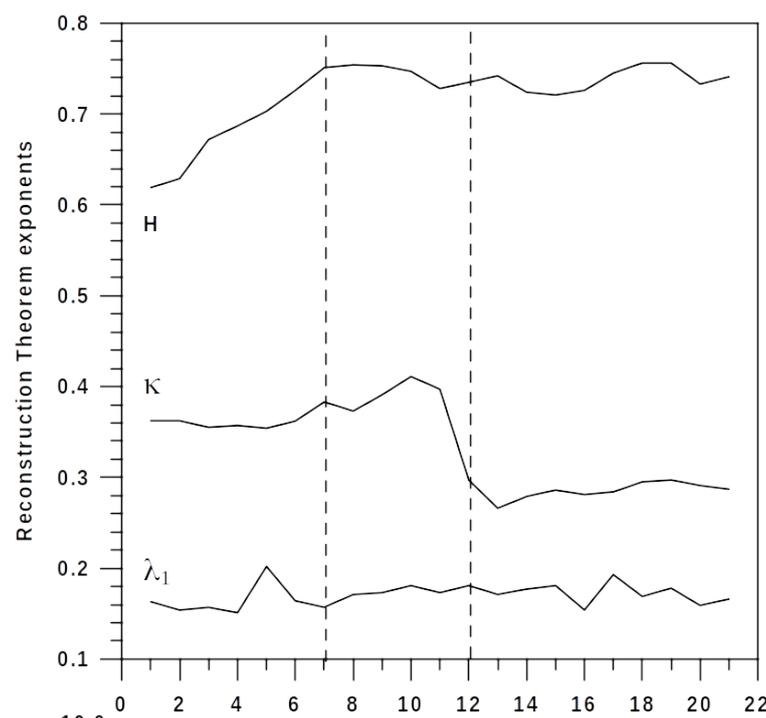
1015

1020

1025

b)
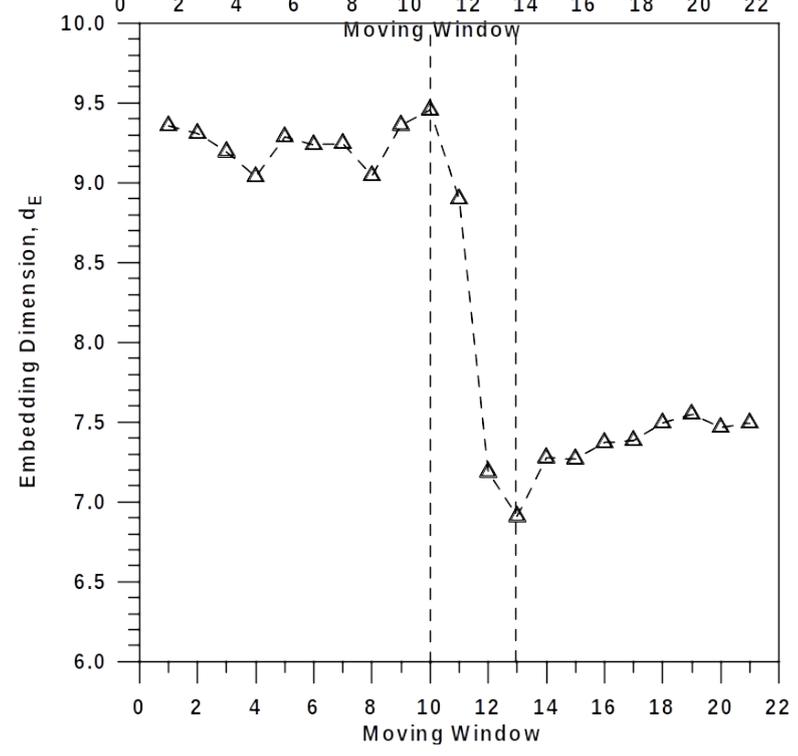
1030

1035

1040

Figure 11. a) Evolution of the Hurst exponent, H, the Kolmogorov entropy exponent, K, and the first Lyapunov exponent, λ_1. b) Embedding dimension d_E, for the 21 moving windows.

1045

Competing interests

The contact author has declared that none of the authors has any competing interests

1050 **Acknowledgments**

The research leading to these results has received funding from the European High-Performance Computing Joint Undertaking (JU) and Spain, Italy, Iceland, Germany, Norway, France, Finland, and Croatia, under grant agreement No. 101093038, ChEESE-2P project

1055 **Data availability**

Data sharing is not applicable to this article as no new data were created or analyzed in this study.